Cell and Tissue Research (2023) 393:537–545
https://doi.org/10.1007/s00441-023-03800-7

REGULAR ARTICLE

Comparative study of calcification in human choroid plexus, pineal gland, and habenula

O. Junemann[1,2] · A. G. Ivanova[3] · I. Bukreeva[1] · D. A. Zolotov[3] · M. Fratini[1,4] · A. Cedola[1] · F. Wilde[5] · I. G. Dyachkova[3] · Yu. S. Krivonosov[3] · D. A. Otlyga[2] · S. V. Saveliev[2]

Received: 23 March 2023 / Accepted: 13 June 2023 / Published online: 24 June 2023

Abstract

Choroid plexus, pineal gland, and habenula tend to accumulate physiologic calcifications (concrements) over a lifetime. However, until now the composition and causes of the intracranial calcifications remain unclear. The detailed analysis of concrements has been done by us using X-ray diffraction analysis (XRD), X-ray diffraction topography (XRDT), micro-CT, X-ray phase-contrast tomography (XPCT), as well as histology and immunohistochemistry (IHC). By combining physical (XRD) and biochemical (IHC) methods, we identified inorganic (hydroxyapatite) and organic (vimentin) components of the concrements. Via XPCT, XRDT, histological, and IHC methods, we assessed the structure of concrements within their appropriate tissue environment in both two and three dimensions. The study found that hydroxyapatite was a major component of all calcified depositions. It should be noted, however, that the concrements displayed distinctive characteristics corresponding to each specific structure of the brain. As a result, our study provides a basis for assessing the pathological and physiological changes that occur in brain structure containing calcifications.

Keywords Choroid plexus · Pineal gland · Habenula · Immunohistochemistry · X-ray diffraction analysis · X-ray phase contrast tomography

Introduction

The calcification of the human brain structures, such as the choroid plexus (ChP), pineal gland (PG), and habenula (HA), is a normal physiological process associated with aging. Furthermore, the calcified deposits may also be involved in pathological processes related to neurodegenerative and mental diseases (Bersani et al. 1999; Kunz et al. 1999; Sandyk 1992; Serot et al. 2003). Since the formation of brain concrements is a dynamic process (Bukreeva et al. 2022), the information about the composition of concrements in normal aging provides a basis to studies of both normal and pathological changes in brain structures. Our research focused on brain structures that are highly synthetically active and are interconnected (very closely in the case of the pineal gland and habenula) but form a different type of concrements.

Pineal gland is a part of circadian rhythm regulation system in the brain. It is composed mainly of pinealocytes, which secrete serotonin during the day and melatonin at night. PG calcium deposits reduce active parenchymal volume that might be associated with sleep disorders, cancer, and several psychiatric and neurodegenerative diseases (Kunz et al. 1999; Bruno et al. 2019; Song 2019; Tan et al. 2018). The growth patterns of human pineal concrements were described by Kim et al. (2012). Of particular interest is the fact that in neoplasms in the pineal gland are formed concrements consisting of amorphous calcium phosphate, which are not detected in the normal aging (Møller et al. 1979).

✉ O. Junemann
junemann@outlook.com

✉ I. Bukreeva
inna.bukreeva@cnr.it

1 Institute of Nanotechnology—CNR (Rome unit), c/o Department of Physics, La Sapienza University, Piazzale Aldo Moro 5, Rome, Italy

2 Avtsyn Research Institute of Human Morphology of Federal State Budgetary Scientific Institution "Petrovsky National Research Centre of Surgery", Tsyurupy Street, 3, Moscow, Russian Federation

3 Federal Scientific Research Centre "Crystallography and Photonics", Russian Academy of Sciences, Leninskiy Prospekt 59, Moscow, Russian Federation

4 IRCCS Santa Lucia Foundation, Via Ardeatina 352, Rome, Italy

5 Institute of Materials Physics, Helmholtz-Zentrum Hereon, Max-Planck-Str. 1, 21502 Geesthacht, Germany

HA plays a central role in the regulation of the human limbic system. Hu et al. suggested that HA, along with PG, is co-involved in the control of the normal sleep–wake cycle (Hu et al. 2020). Some researchers revealed a link between calcifications in HA and neurodegenerative diseases (Sandyk 1992).

ChP is a villous epithelial–endothelial vascular structure within the ventricular system of the vertebrate brain. The ChP, primarily responsible for the secretion of cerebrospinal fluid, is involved in a variety of neurological disorders, including neurodegenerative disorders (Serot et al. 2003), and inflammatory, infectious, traumatic, neoplastic, and systemic diseases (Bersani et al. 1999; Wolburg and Paulus 2010).

The chemical compositions of PG and ChP concrements have been extensively studied. The researchers generally reported about the PG concretions, which consist mainly of hydroxyapatite (Mabie and Wallace 1974; Kodaka et al. 1994). In addition to calcium, some other elements (iron, copper, zinc, magnesium) were found as well (Michotte et al. 1977a, b). Some controversial data on the chemical composition of psammoma bodies (ChP concrements) was published in the literature. Several authors assumed that psammoma bodies, like PG concrements, are the calcified deposits that may contain zinc, iron, magnesium, manganese, copper besides calcium as well (Macpherson and Matheson 1979; Modic et al. 1980; Michotte et al. 1977a, b (2)). Other researchers supposed that the source of psammoma bodies was meningocytes forming whorls in the stroma of ChP, which are later impregnated with calcium salts (Shuangshoti and Netsky 1970).

Our research provides the study of the concrement composition and morphology in human post-mortem PG, HA, and ChP. The detailed analysis of concrements was done using X-ray diffraction analysis (XRD), X-ray diffraction topography (XRDT), micro-CT, X-ray phase-contrast tomography (XPCT), as well as histology and immunohistochemistry (IHC). We have observed that the brain concrements frequently have a concentric layered morphology, but they exhibit a wide variation in layer configuration. We have found that the concrements in all three studied brain structures contain hydroxyapatite. However, PG concrements have no organic matrix, while HA concrements may include an organic core and alternating layers of ChP concrements containing calcified and noncalcified organic material with vimentin as its main organic component. Our work provides a basis for prospective studies on calcified brain structures to gain insight into the mechanisms of brain calcification and how they affect nervous system function in human.

Materials and methods

Samples

The material for the study were PGs, Has, and ChPs taken from human autopsies and included 25 samples of the choroid plexus, 35 samples of the pineal gland, and 9 samples of the habenula (from 27 to 96 years old). The tissue samples were taken after 12–24 h after the death and fixed 24–30 h in 10% neutral buffered formalin. After that they were dehydrated in eight portions of isopropyl alcohol and embedded in paraffin. The 30 samples were measured via micro-CT and XP-CT prior to histological analysis. Histological study was performed on 25 samples of ChP, 30 samples of PG, and 6 samples of HA. XRDT experiments were carried out on two kinds of samples: (1) the first sample was a whole uncut PG (PG parenchyma with calcification) embedded in paraffin; (2) in the second experiment, three independent concrements were extracted from ChP, PG, and HA, one for each brain structure.

XRD analysis was done on the concrement samples (12 in total) collected from ChP (5 samples), PG (6 samples), and HA (3 samples).

Micro-CT, XPCT, and XRDT experiments with whole PGs, as well as histological and IHC analyses, were performed on samples fixed in 10% formalin. The samples of PG, HA, and ChP for XRD and XRDT experiments were fixed and kept in 70% alcohol. Before the experiment, the calcifications were extracted from the tissue. The sample description is summarized in Table S1 in Supplementary information.

Micro-computed tomography (micro-CT), X-ray phase contrast tomography (XPCT)

Micro-CT and XPCT (see Supplementary information) provided us the whole-sample 3D images of PG, ChP, and HA. Laboratory micro-CT setup was used to select samples containing calcified concrements, which were then analyzed by other methods. We used synchrotron-based XPCT free space propagation setup (Snigirev et al. 1995) to image the samples (see Supplementary information, Fig. S6). This technique enabled 3D imaging of morphological structures of soft tissue invisible to micro-CT.

Micro-CT scans were carried out at laboratory microtomography setup "TOMAS." The accelerating voltage and current were 45 kV and 40 mA, respectively. X-ray beam energy was 17.5 keV (pyrographite crystal was used as a monochromator). Tomographic scans were performed using 1000 X-ray projected images with an angular range of 200° and a step of 0.5°. For the entire sample, the scan took about 100 min. The XIMEA xiRAY11 detector (Buzmakov et al. 2018) pixel size was of 9×9 micron^2.

After micro-CT experiment the selected samples were measured via XPCT at the P05 beamline of the synchrotron facility PETRA III, DESY, operated by the Helmholtz-Zentrum Hereon (PETRA III, DESY) (Wilde et al. 2016; Khokhriakov et al. 2017) using a monochromatic beam energy 25 keV. The set of tomographic projections was

acquired in half-acquisition mode (Vo et al. 2021) with 4000 projections and an exposure time of 0.25 s, covering a total angle range of 360°. The sample was placed at a distance of 50 cm from the recording system with pixel sizes 1.28×1.28 micron^2 and 0.64×0.64 micron^2.

Micro-CT and XPCT data processing

The X-ray projected images were pre-processed using dark field and flat field corrections, as well as Raven filters for ring removal (Raven 1998). The CGLS algebraic method (Chukalina et al. 2019) was applied for tomographic reconstruction of micro-CT data. MatLab package (Moosmann et al. 2014) was used to perform the pre-processing and phase and tomographic reconstructions of the XPCT data. For the reconstruction of X-ray phase-contrast tomograms, filtered back projection with a linear ramp filter has been used. In reconstructed tomography images, grayscale variations indicate changes in absorption coefficients (absorption contrast) or electron densities (phase contrast). Tools and plugins of the open-source programs ImageJ/Fiji (Schindelin et al. 2012) were used to visualize the data.

X-ray diffraction analysis (XRD)

The main aim of our XRD-based study was to identify the major mineral constituents of concrement in ChP, PG, and HA. XRD patterns of concrements extracted from PG, HA, and ChP were recorded on the XCalibur Eos S2 (Rigaku Oxford diffraction, Japan) diffractometer in transmission geometry (Debye–Scherrer) using monochromatic MoKα1 radiation ($\lambda = 0.7093$ Å, 50 kV, 40 mA, beam size 500×500 μm^2) and CCD detector EOS S2. The sample-detector distance was 41.5 mm and the exposure time was 40 min. Integration of two-dimensional diffraction patterns and transformation to one-dimensional form were carried out using CrysAlisPro software (Rigaku Oxford Diffraction 2019). The phase identification was performed using the PDXL program (Rigaku Corporation, Japan) and ICDD PDF-2 datasets (release 2017).

X-ray diffraction analysis (XRDT)

We used XRDT (see Figs. S2–S5 Supplementary information) for a non-destructive structural research of individual crystalline elements (grains or subgrains) in the bulk of polycrystals (concrements).

The samples from each studied brain structure were measured on a laboratory X-ray diffractometer "DITOM-M." X-ray tube with a molybdenum anode was used as a source of X-ray polychromatic radiation. The electric current in an X-ray tube operating at 40 kV was 40 mA. The beam was formed by a pair of mutually perpendicular slits and had a dimension 1.5×1.5 mm^2. Diffraction patterns were recorded using a Ximea XiRay11 2D detector with a field of view of 36×29 mm^2 and a pixel size of 9×9 μm^2. A total of 1800 projections were measured for all samples in the rotation range from 0 to 180° with an angular step of 0.1°. The time to obtain one frame was 60 s.

XRDT data processing

The projection images were first processed by median filter (with a window size of 3×3 pixels) correction through the image stack for all angles of rotation to remove the background noise. After the filtering procedure all images from the stack were combined in an integrated image, each of whose pixels contained the maximum value over all images in the stack at the particular pixel location (maximum intensity projection). The integrated image was used to analyze crystalline elements (grains or subgrains) of concrements.

Histology and IHC

Paraffin-embedded tissue blocks were cut and the sections of 10 micron thick were prepared for histological and IHC analyses. Mallory method was used for detection of connective tissue. Antibodies to collagens type I-V and vimentin were used to detect the organic part of concrements. The other tissues (pia mater, cartilage) from the same persons were used as positive controls. The names of antibodies and conditions of IHC reactions are provided in Table S2 in Supplementary information. The Ultra Vision LP Detection System of the firm Thermo Scientific (catalog Nr. TL-125-HD) was used as the second antibodies. To exclude non-specific staining by secondary antibodies, negative controls were performed to displace the primary antibody with PBS buffer (Fig. S1 in Supplementary information).

Results and discussion

Micro-CT, XRDT, XRD analysis

XRDT technique revealed that all PG samples contain polycrystals with grain sizes up to 100 microns, with an average value of 20–30 microns (see Figs. S2–S5 in Supplementary information).

XRD analysis allowed us to identify the crystalline phases in the concrements of PG, ChP, and HA. The crystalline phase composition was determined by comparing the acquired data with those in reference databases.

Figure 1 illustrates the results of the XRD analysis for the typical samples of PG (Fig. 1a, a′), HA (Fig. 1b, b′), and ChP (Fig. 1c, c′) concrements. Two-dimensional XRD images and the corresponding integrated one-dimensional XRD patterns are shown in Fig. 1a–c and a′–c′, respectively. Microphotographs

of the concrements are shown in Fig. 1a′–c′. XRD pattern showed characteristic peaks corresponding to hydroxyapatite $Ca_5(PO_4)_3(OH)$ (PDF#1–084-1998) (Hughes et al. 1989) for all concrements under investigation (PG, HA, and ChP).

The summary graph representing XRD patterns for all studied brain structures is shown in Fig. 2. The experimental diffraction patterns of concrements in PG (blue lines), HA (green lines), and ChP (red lines) match with the XRD patterns simulated using crystal structure of hydroxyapatite $Ca_5(PO_4)_3(OH)$ (ICSD#203,027) with the instrumental broadening of the diffractometer (black line). According to XRD, concrements in PG and HA are primarily composed of crystalline hydroxyapatite, while the calcified concrements in ChP appear to be predominantly composed of hydroxyapatite with a low degree of crystallinity.

Histological, IHC, and XPCT analysis

Pineal gland

The internal structure of PG was investigated in 2D and 3D via histological and XPCT imaging, respectively. We

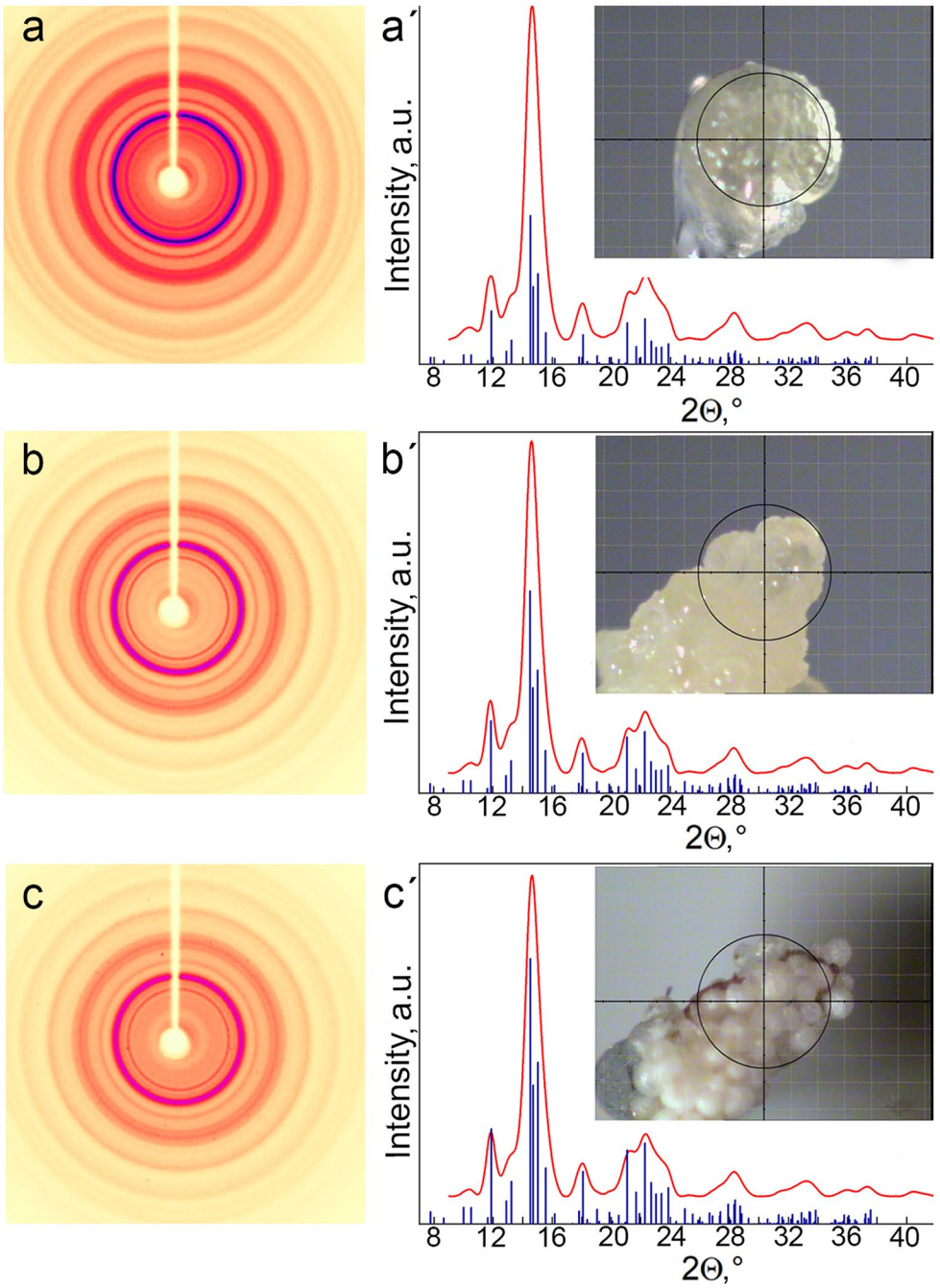

Fig. 1 X-ray diffraction patterns of **a**, **a′** PG, **b**, **b′** HA, and **c**, **c′** ChP concrements. Two-dimensional XRD images and the corresponding integrated one-dimensional XRD patterns are **a**–**c** and **a′**–**c′**, respectively. Microphotographs of the concrements are shown in **a′**–**c′**. All structures showed characteristic peaks (in red) corresponding to the reflections of hydroxyapatite (in blue)

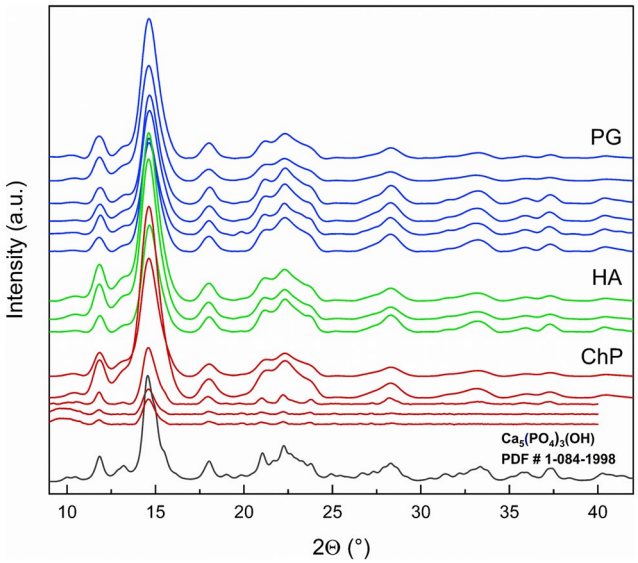

Fig. 2 Summary graph of the XRD experiments. XRD patterns of PG concrements (blue), HA concrements (green), and ChP concrements (red). The simulated XRD pattern of hydroxyapatite $Ca_5(PO_4)_3(OH)$ (ICSD#203027) (Hughes et al. 1989) is shown in black

identified concrements with different shapes and internal structure. In particular, we found laminated and aggregated calcified deposits. The histological images of laminated concrements and volumetric XPCT image of aggregated solid concrements are shown in Fig. 3a and b, respectively. Additionally, we observed the mulberry-like conglomerates developed as a result of aggregation of numerous agglomerated nodes. The volumetric XPCT image of PG calcified conglomerate is shown in Fig. 3c. We note that the large-scale PG calcifications were visualized with XPCT imaging since large concrements are commonly broken during histological treatment, making the analysis problematic. Moreover, decalcification during histological sample preparation can impair the staining of the tissues.

Habenula

A common finding in HA is small concrements that have not formed conglomerates. Volumetric XPCT image of PG with highly calcified HA is shown in Fig. 4a. Image contrast in the figure was adjusted to visualize the calcified tissue. The white double arrow at the top of the figure points to the group of concrement in HA. The single white arrow at the central part points to large mulberry-like conglomerates in PG. Figure 4b shows the histological section of HA with a laminated concrement. Concrements in HA occasionally have loose core zones, unlike those in PG.

Via XPCT-based study we readily identified PG and HA as distinct structures with well-visible separation between them, even in case when these structures were completely calcified (see Fig. 4a). This implies that concrements were formed independently in PG and HA, but they shared a common mechanism of formation. This assumption is confirmed by Vigh et al. (1998), where the biochemical basis of this process is described in detail. Our finding suggests that the formation of calcified deposits in different brain structures should be considered structure specific and can be categorized based on the morphology and composition of concrements.

Electron microscopy-based investigation showed that the calcifications of PG begin within cells. Small crystals have been detected in several cell organelles of PG in Lewczuk et al. (1994). Our histological and XPCT examinations revealed some additional aspects of concrement formation. According to our research, after the onset of calcification, layers are deposited around the primary center, forming individual concrements that can later fuse together to form larger conglomerates (see Fig. 3). Interesting results were obtained by A. Novier and co-authors in the study of the calcium-binding protein calretinin. The authors assume that this protein participates in the formation of pineal gland concretions (Novier et al. 1996). In some cases we detected the concrements in PG near of the

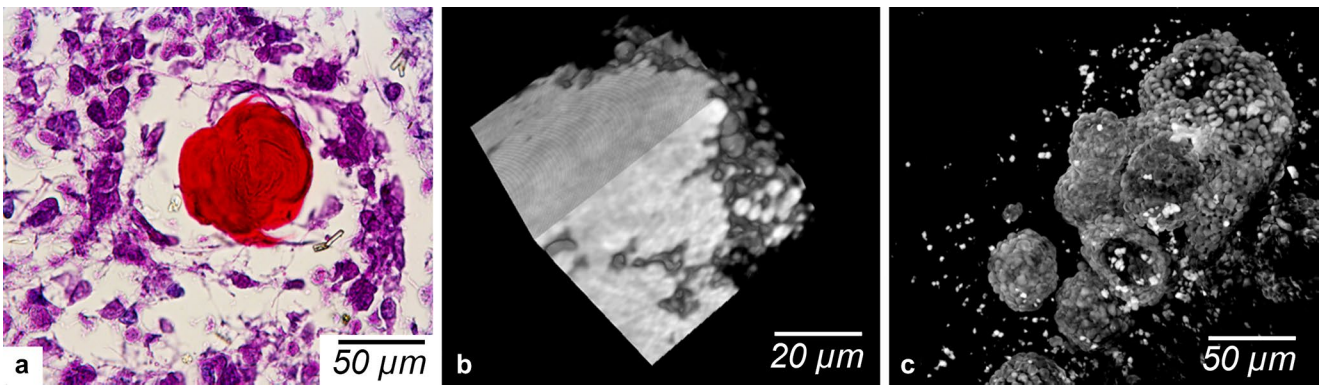

Fig. 3 PG concrements (female, 41 y.o.). **a** Histological image of small single laminated concrement, Mallory staining; **b** XPCT volumetric image of aggregated solid calcified concretion; **c** XPCT volumetric image of large mulberry-like calcified conglomerates

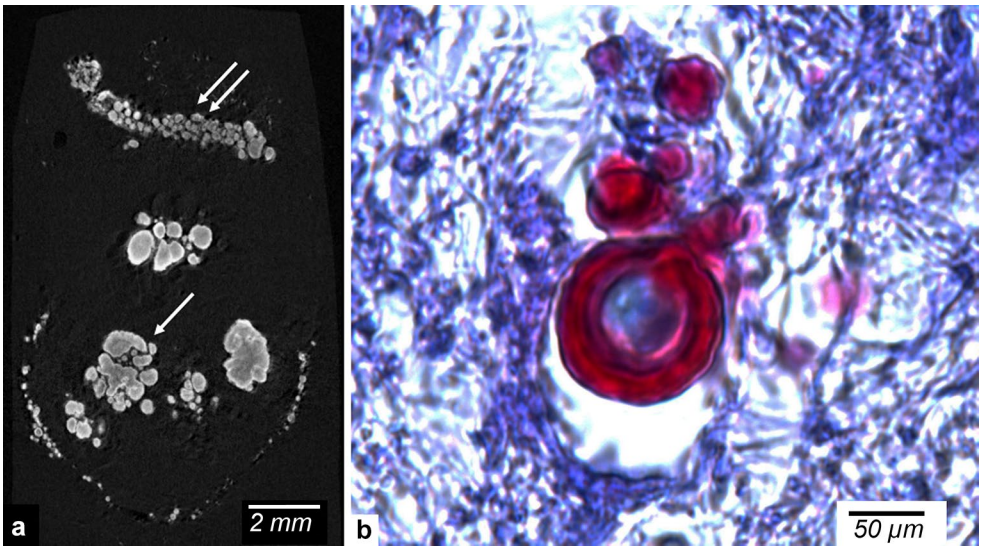

Fig. 4 Habenula concrements. **a** XPCT slice image of small independently developed concrements in HA shown with white double arrow, the single white arrow points to calcified conglomerates in PG (male, 62 y.o.); **b** histological image of HA tissue (female, 47 y.o.) with concrements (Mallory staining); loose core zones are visible

calcified stroma and blood vessels (Bukreeva et al. 2022). The connection between the calcification processes in blood vessels and parenchyma cannot be excluded. Calcification of blood vessels is described in detail by Maheshwari et al. (2022).

In our study, some HA concrements showed a loose core (Fig. 4b). This may indicate the presence of an organic fraction in the core formed by dead cells, which are later impregnated with calcium salts, in particular, with hydroxyapatite. On the other hand, some HA concrements showed no structural differences from the PG concrements. Therefore, the concrements in HA may actually be two different types: one organic as is typical of HA only and the other without organic substances, which occurs in both PG and HA.

Choroid plexus

XRD analysis of ChP calcifications revealed hydroxyapatite peaks, as observed for both PG and HA (see Figs. 1 and 2). However, histological and XPCT examination detected significant differences in the morphological organization of concrements in ChP compared to other brain structures under our study. Figure 5 shows different types of ChP concrements. They usually have a round layered structure and never seem to form conglomerates; however, as illustrated in Fig. 5a, b, they show great variety in the organization of their layers. Figure 5c illustrates XPCT slice image of ChP with a variety of concrements.

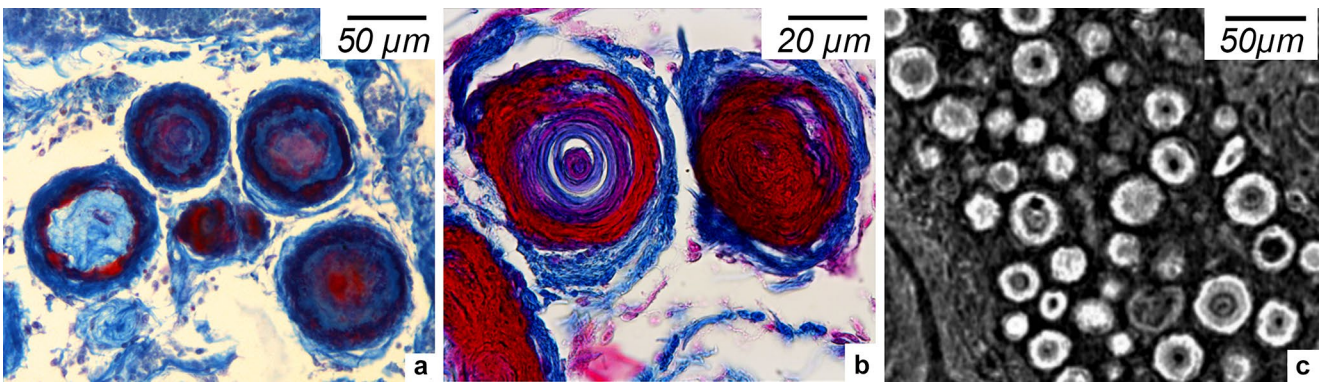

Fig. 5 Different types of ChP concrements (female, 70 y.o.). **a**, **b** Histological image, Mallory staining; **a** concrements with an alternation of calcified and noncalcified layers; **b** layers are calcified only on the outer surface of the concrements or calcified core of the concrements; **c** different types of concrements in XPCT slice image

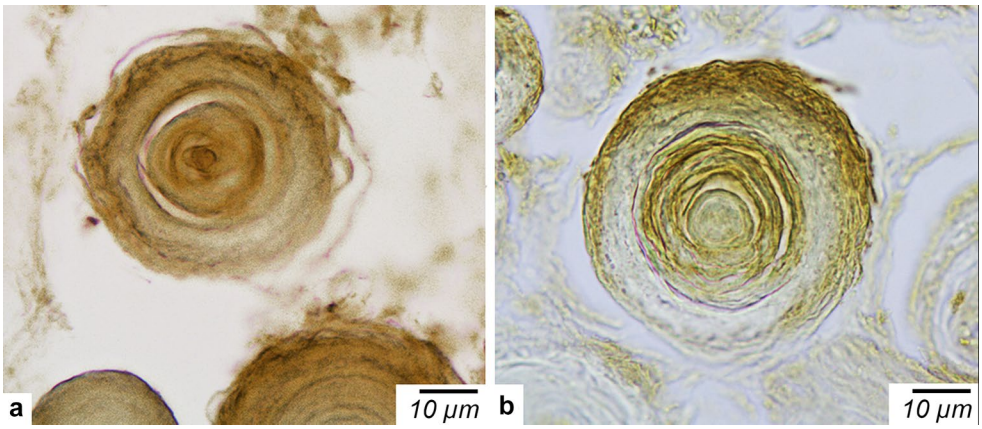

Fig. 6 IHC analysis of ChP tissue from male, 46 y.o with the antibodies to vimentin. **a** Immunopositive core zone of the concrements was observed. **b** Alternation of immunopositive and immunonegative layers is clearly visible

The number of concrements in each brain structure studied ranges from nearly completely calcified tissues (in case of PG and HA) to ones without concrements. Figures 3, 4, and 5 illustrate one of the typical states of these structures.

Figure 6 illustrates the IHC analysis of two different ChP tissue parts from male 46 years old. Some layers of the concrements show clear presence of vimentin. Collagens of I, II, III, IV, and V types were not detected in concrements.

Different types of concrements were found in villi of ChP; they underplayed the epithelial cell layer (see Fig. 7a, b). The concrements are also clearly seen in XPCT slice image (Fig. 7c). IHC analysis of Fig. 7 suggests that they are composed of collagen III (Fig. 7a) or IV type (Fig. 7b).

ChP produces a specific type of concrements which contain an organic, fibrous component. Although some articles claimed that collagen in ChP calcification was present, no evidence of this was found in our research. According to our IHC analysis, vimentin formed only some layers of the concrements, which corresponds to results reported in Korzhevskii (1997). The remaining layers of the concrements appeared calcified, which can be also clearly seen in XPCT images (Fig. 5c). The way in which calcium salt impregnates these layers cannot be fully understood, given the diversity of concrement configuration (Fig. 5). In particular, we found that the most common morphological structure of calcification in ChP was the alternation of calcified and noncalcified layers (Fig. 5a). On the other hand, in some ChPs, calcium-rich layers formed only the outer surface of concrements (Fig. 5b), while in other ChPs calcified layers were observed only in the central part of the concrements (Fig. 5c).

Among the concrements observed in ChP, there were subepithelial thicknesses that underlay the epithelial cell layer (Fig. 7). These types of concrements are well visible in XPCT images. We assume that it can be collagen IV (Fig. 7b), which causes basement membrane edema, or collagen III (Fig. 7a), which leads to stromal compression. It is worth noting that even if calcium salt impregnation has not been proven, it could not be completely excluded.

Fig. 7 Villi of ChP. **a** IHC staining with the antibodies to collagen III (male, 62 y.o.); **b** IHC staining with the antibodies to collagen IV (female, 59 y.o.); **c** XPCT slice image (female, 59 y.o.). Concrements are shown with red arrows

Conclusion

Physiologic calcifications in ChP, PG, and HA from human autopsies were analyzed with combination of complementary methods. XRD indicates that PG and HA concrements are primarily composed of crystalline hydroxyapatite, whereas calcified concrements of ChP contain mostly hydroxyapatite with a low degree of crystallinity. Based on multi-technique approach, we have found that the concrements displayed distinct morphological and chemical characteristics for each brain structure. Accordingly, we believe that our findings may provide a useful basis for study of physiologic and pathological processes in human brain.

Supplementary Information The online version contains supplementary material available at https://doi.org/10.1007/s00441-023-03800-7.

Acknowledgements X-ray diffraction experiments were performed within the State assignment of FSRC "Crystallography and Photonics" of Russian Academy of Sciences using the equipment of the Shared Research Center FSRC "Crystallography and Photonics" RAS. This work was performed within the State Assignment of FSRC "Crystallography and Photonics" RAS in part of X-ray studies.

Author contribution O.J. and S.V.S. conceived and designed the research; O.J. and D.A.O. performed the research and acquired the histological and IHC data; A.G.I. performed the research and acquired the XRD data; I.B., M.F., A.C., and F.W. performed the research and acquired the XPCT data; D.A.Z., I.G.D., and Yu.S.K. performed the research and acquired the XRDT data; O.J., S.V.S., I.B., A.G.I., and D.A.Z. analyzed and interpreted the data. All authors were involved in drafting and revising the manuscript.

Data availability The data that support the findings (histological, IHC, XRD, XRDT, XPCT) of this study are available on request from the corresponding author.

Declarations

Ethical approval The study was carried out on autopsy material obtained from the collection of Federal State Scientific Institution Research Institute of Human Morphology (Moscow, Russian Federation). All protocols were approved by the Ethical Committee of the Research Institute of Human Morphology of the Russian Academy of Medical Sciences (now FSSI Research Institute of Human Morphology) (No. 6A of October 19, 2009) and are in correspondence with instructions of the Declaration of Helsinki including points 7–10 for human material from 12.01.1996 with the last amendments from 19.12.2016.

Consent to participate Not applicable.

Conflict of interest The authors declare no competing interest.

References

Bersani G, Garavini A, Taddei I, Tanfani G, Pancheria P (1999) Choroid plexus calcification as a possible clue of serotonin implication in schizophrenia. Neurosci Lett 259:169–172. https://doi.org/10.1016/S0304-3940(98)00935-5

Bruno F, Arrigoni F, Maggialetti N, Natella R, Reginelli A, Di Cesare E, Brunese L, Giovagnoni A, Masciocchi C, Splendiani A, Barile A (2019) Neuroimaging in emergency: a review of possible role of pineal gland disease. Gland Surg 8. https://doi.org/10.21037/gs.2019.01.02

Bukreeva I, Junemann O, Cedola A, Brun F, Longo E, Tromba G, Wilde F, Chukalina MV, Krivonosov YS, Dyachkova IG, Buzmakov AV, Zolotov DA, Palermo F, Gigli G, Otlyga DA, Saveliev SV, Fratini M, Asadchikov VE (2022) Micro-morphology of pineal gland calcification in age-related neurodegenerative diseases. Med Phys. https://doi.org/10.1002/mp.16080

Buzmakov AV, Asadchikov VE, Zolotov DA, Roshchin BS, Dymshits YuM, Shishkov VA, Chukalina MV, Ingacheva AS, Ichalova DE, Krivonosov YuS, Dyachkova IG, Balzer M, Castele M, Chilingaryan S, Kopmann, (2018) A Laboratory microtomographs: design and data processing algorithms. Crystallogr Reports 63:1057–1061. https://doi.org/10.1134/S106377451806007X

Chukalina MV, Ingacheva AS, Buzmakov AV, Krivonosov YS, Asadchikov VE, Nikolaev DP (2019) A hardware and software system for tomographic research: reconstruction via regularization. Bull Russ Acad Sci Phys 83:150–154. https://doi.org/10.3103/S1062873819020084

Hu H, Cui Y, Yang Y (2020) Circuits and functions of the lateral habenula in health and in disease. Nat Rev Neurosci 21:277–295. https://doi.org/10.1038/s41583-020-0292-4

Hughes JM, Cameron M, Crowley KD (1989) Structural variations in natural F, OH, and Cl apatites. Am Miner 74:870–876

Khokhriakov I, Beckmann F, Lottermoser L (2017) Integrated control system environment for high-throughput tomography, Proc. SPIE 10391, Developments in X-Ray Tomography XI, 103911H1–10. https://doi.org/10.1117/12.2275863

Kim J, Kim HW, Chang S, Kim JW, Je JH, Rhyu IJ (2012) Growth patterns for acervuli in human pineal gland. Sci Rep 2:984. https://doi.org/10.1038/srep00984

Kodaka T, Mori R, Debari K, Yamada M (1994) Scanning electron microscopy and electron probe microanalysis studies of human pineal concretions. J Electron Microsc 43:307–317. https://doi.org/10.1093/oxfordjournals.jmicro.a051117

Korzhevskii DE (1997) The formation of psammoma bodies in the choroid plexus of the human brain. Morfologiia 111:46–49. PMID: 9244548

Kunz D, Schmitz S, Mahlberg R, Mohr A, Stöter C, Wolf K-J, Herrmann WM (1999) A new concept for melatonin deficit: on pineal calcification and melatonin excretion. Neuropsychopharmacology 21:765–772. https://doi.org/10.1016/S0893-133X(99)00069-X

Lewczuk B, Przybylska B, Wyrzykowski Z (1994) Distribution of calcified concretions and calcium ions in the pig pineal gland. Folia Histochem Cytobiol 32:243–249. PMID: 7758619

Mabie CP, Wallace BM (1974) Optical, physical and chemical properties of pineal gland calcifications. Calc Tis Res 16:59–71. https://doi.org/10.1007/BF02008213

Macpherson P, Matheson MS (1979) Comparison of calcification of pineal, habenular commissure and choroid plexus on plain films and computed tomography. Neuroradiology 18:67–72. https://doi.org/10.1007/BF00344824

Maheshwari U, Huang SF, Sridhar S, Keller A (2022) The interplay between brain vascular calcification and microglia. Front Aging Neurosci 14:1–14. https://doi.org/10.3389/fnagi.2022.848495

Michotte Y, Lowenthal A, Knaepen L, Collard M, Massart DL (1977a) A morphological and chemical study of calcification of the pineal gland. J Neurol 215:209–219. https://doi.org/10.1007/BF00312479

Michotte Y, Massart DL, Lowenthal A, Knaepen L, Pelsmaekers J, Collard M (1977b) Morphological and chemical study of calcification of the choroid plexus. J Neurol 216:127–133. https://doi.org/10.1007/BF00312946

Modic MT, Weinstein MA, Rother AD, Erenberg G, Duchesneau PM, Kaufman B (1980) Calcification of the choroid plexus visualized by computed tomography. Radiology 135:369–372. https://doi.org/10.1148/radiology.135.2.7367628

Møller M, Gjerris F, Hansen HJ, Johnson E (1979) Calcification in a pineal tumour studied by transmission electron microscopy, electron diffraction and x-ray microanalysis. Acta Neurol Scand 59(4):178–187. https://doi.org/10.1111/j.1600-0404.1979.tb02928.x

Moosmann J, Ershov A, Weinhardt V, Baumbach T, Prasad MS, LaBonne C, Xiao X, Kashef HR (2014) Time-lapse X-ray phase-contrast microtomography for in vivo imaging and analysis of morphogenesis. Nat Protoc 9:294–304. https://doi.org/10.1038/nprot.2014.033

Novier A, Nicolas D, Krstic R (1996) Calretinin immunoreactivity in pineal gland of different mammals including man. J Pineal Res 21:121–130. https://doi.org/10.1111/j.1600-079x.1996.tb00279.x

Raven C (1998) Numerical removal of ring artifacts in microtomography. Am Inst Phys 69:2978–2980. https://doi.org/10.1063/1.1149043

Rigaku Oxford Diffraction (2019) CrysAlisPro Software System. Version. 1.171.39.46 (Wroclaw, Poland)

Sandyk R (1992) Pineal and habenula calcification in Schizophrenia. Int J Neurosci 67:19–30. https://doi.org/10.3109/00207459208994773

Schindelin J, Arganda-Carreras I, Frise E, Kaynig V, Longair M, Pietzsch T, Preibisch S, Rueden C, Saalfeld S, Schmid B, Tinevez J-Y, White DJ, Hartenstein V, Eliceiri K, Tomancak P, Cardona A (2012) Fiji: an open-source platform for biological-image analysis. Nat Methods 9:676–682. https://doi.org/10.1038/nmeth.2019

Serot J-M, Bene M-C, Faure GC (2003) Choroid plexus, ageing of the brain, and Alzheimer's disease. Front Biosci 8:515–521. https://doi.org/10.2741/1085

Shuangshoti S, Netsky M (1970) Human choroid plexus: morphologic and histochemical alteration with age. Am J Anat 128:73–96. https://doi.org/10.1002/aja.1001280107

Song J (2019) Pineal gland dysfunction in Alzheimer's disease: relationship with the immune-pineal axis, sleep disturbance, and neurogenesis. Mol Neurodegener. https://doi.org/10.1186/s13024-019-0330-8

Snigirev A, Snigireva I, Kohn V, Kuznetsov S, Schelokov I (1995) On the possibilities of x-ray phase contrast microimaging by coherent high-energy synchrotron radiation. Rev Sci Instrum 66:5486–5492. https://doi.org/10.1063/1.1146073

Tan D, Xu B, Zhou X, Reiter RJ (2018) Pineal calcification, melatonin production, aging, associated health consequences and rejuvenation of the pineal gland. Molecules 23:301. https://doi.org/10.3390/molecules23020301

Vigh B, Szél A, Debreceni K, Fejér Z, Manzano e Silva MJ, Vigh Teichmann I (1998) Comparative histology of pineal calcification. Histol Histopathol 13:851–870

Vo NT, Atwood RC, Drakopoulos M, Connolley T (2021) Data processing methods and data acquisition for samples larger than the field of view in parallel-beam tomography. Opt Express 29:17849–17874. https://doi.org/10.1364/OE.418448

Wilde F, Ogurreck M, Greving I, Hammel JU, Beckmann F, Hipp A, Lottermoser L, Khokhriakov I, Lytaev P, Dose T, Burmester H, Müller M, Schreyer A (2016) Micro-CT at the imaging beamline P05 at PETRA III. AIP Conf Proc. https://doi.org/10.1063/1.4952858

Wolburg H, Paulus W (2010) Choroid plexus: biology and pathology. Acta Neuropathol 119:75–88. https://doi.org/10.1007/s00401-009-0627-8